EREM 77/2
Journal of Environmental Research, Engineering and Management
Vol. 77 / No. 2 / 2021
pp. 111–110
DOI 10.5755/10.5755/j01.erem.77.2.28286

Numerical Analysis of Optimizing a Heat Sink and Nanofluid Concentration Used in a Thermoelectric Solar Still: an Economic and Environmental Study

Received 2021/01 | Accepted after revision 2021/04

http://dx.doi.org/10.5755/j01.erem.77.2.28286

Numerical Analysis of Optimizing a Heat Sink and Nanofluid Concentration Used in a Thermoelectric Solar Still: an Economic and Environmental Study

Shahin Shoeibi*

Department of mechanical engineering, Semnan Branch, Islamic Azad University, Semnan, Iran

***Corresponding author:** shsh238@yahoo.com

In this paper, mathematical modelling is performed for a group of fins in a heat sink in order to determine the optimum dimensionless thickness of the fins using 8 different types of cooling nanofluids including nanoparticles of aluminium, alumina, titanium, titanium dioxide, copper, copper oxide, iron and iron oxide (hematite) with water as the base fluid in a thermoelectric solar still. The heat sink is used to enhance thermoelectric cooling and heating to water. The flow crossing fins is considered laminar and fully developed. Copper with high thermal conductivity is considered as the material of flat plate fins. Different nanofluids with volume fractions of 1%, 3%, 5%, 7% and 9% with a nanoparticle diameter of 25, 50 and 75 nm are analyzed for fins with rectangular cross sections. Besides, the economic and environmental analysis is conducted on the thermoelectric solar still. It is also observed that the range of 3.65% to 3.95% is obtained for the optimum volume fraction in the used nanofluids. The carbon dioxide mitigation based on the environmental parameter and exergoenvironmental parameters in the solar still is about 23.78 tons of CO_2 and 1.04 tons of CO_2, respectively.

Keywords: nanoparticles, heat sink, nanofluid, thermoelectric, solar still.

Introduction

In recent years, many studies have been done about cooling of fluid and some of them concerning heat transfer using fins in heat sinks. Conventional methods for increasing heat transfer consist of increasing the heat transfer area of fins (Shoeibi et al., 2020), adding the number of fins or changing their geometrical shape, and a combination of these methods. Many designs have been conducted to use various nanoparticles to improve the performance of a solar still (Sahota et al., 2017a; Faizal et al., 2013; Singh, 2008b). The main goal for researchers in this field is to keep the temperature of electronic parts in the allowable range, since in case of increasing their temperature more than the allowable range, these parts fail to operate properly and the percentage of errors increases. Therefore, cooling of electronic parts is very essential and important.

Manay and Shahin (2017) experimentally determined the volume fraction upper limitations of the TiO_2–water nanofluid for heat transfer performance in microchannels. They showed that addition of nanoparticles with an average diameter smaller than 25 nm into the base fluid leads to reduction in the thermal resistance. They also indicated that TiO_2–water nanofluid increased heat transfer with a volume fraction up to 2.0%, but heat transfer decreased after that. Xia et al. (2016) investigated convection heat transfer of alumina and titanium dioxide nanofluid in heat sinks. They showed that nanoparticle motion due to convection results in stopping the laminar flow and increasing heat transfer. One of the most important effects of nanofluids is the significant improvement of thermal conductivity (Chen et al., 2017).

The increasing thermal conductivity can be observed even in low concentrations of nanofluids. Various observations (Li and Eastman, 1999; Masuda et al., 1993) proved that having low volumes of nanoparticles (1 to 5 volumetric percent) increased the thermal conductivity of a suspension up to 20%. This increase depends on factors like size of particles, volume in the suspension and thermal properties of particles. Nanofluids have many advantages with respect to usual fluids which make them suitable for heat exchangers (Sahota et al., 2017a). Naphon and Nakharintr (2013) studied heat transfer performance of TiO_2–water nanofluid flowing through a small heat sink with rectangular fins and concluded that the optimized fin geometry reached maximum performance. Zhang et al. (2013) studied heat transfer of Al_2O_3-water nanofluid with volume fractions of 0.25%, 0.51% and 0.77% in a circular microchannel experimentally. They proved that the Nusselt number of Al_2O_3-water nanofluid was higher than pure water, and with enhancement in the Reynolds number and volume fraction of nanoparticles, the Nusselt number increased, too. The highest increment of the Nusselt number is 10.6% and is related to a nanofluid with the concentration of 0.77%.

Using nanoparticles suspended in water with volume fraction concentrations of 0%, 5%, 16% and 31%, Escher et al. proved that increasing concentration had a meaningful effect on the Nusselt number and improved heat transfer in a microchannel (Escher et al., 2011).

Nanofluid is referred to a solution of metallic or non-metallic nanoparticles suspended in a base fluid. For example, blood is a complex bio nanofluid. The super fine particles in a nanofluid change heat transfer properties and result in improvement of heat transfer (Singh, 2008a). Researchers Li and Chao (2009) and Li et al. (2013) have studied heat transfer of flat plate heat sinks, focusing on enhancement of flat plate and circular fin geometry. The results showed that, by increasing flow turbulence, the heat transfer function of flat plate fins improved. Jung et al. (2009) investigated convection heat transfer of Al_2O_3-water nanofluid in a rectangular microchannel in a laminar flow condition. They observed that the heat transfer coefficient for a volume fraction of 1.8% increased by more than 32% with respect to the base fluid. Wen and Ding (2004) investigated the laminar flow of Al_2O_3-water nanofluid in a copper pipe, experimentally. They showed that adding aluminium oxide nanoparticles to water up to 1.6% resulted in an increase of the Nusselt number up to 38%. Many studies have been done regarding the increase of heat transfer in a parallel flow for enhancement of flat plate and circular fin geometry.

In this research, optimizing the thickness of flat plate fins used in a heat sink of a solar still in order to maximize heat transfer for different nanofluids with different volume fractions and nanoparticle diameters was studied. The main aim of this study is to find the effect of different

nanofluids in designing the optimum geometry of fins and to determine fin thickness to obtain more heat transfer. To achieve this goal, using mathematical modelling, the energy equation for a flat plate fin with an insulated end is solved to obtain the heat transfer rate, and then by maximizing it, the optimum fin thickness is calculated. Finally, the economic and environmental analysis of a thermoelectric solar still was conducted.

Material and methods

In this study, both thermoelectric hot and cold sides are connected to two cooling and heating tanks, which are used to decrease the glass temperature from the cold side and raise the water temperature from the hot side of the solar still, shown in Fig 1. The solar still was tested in the climatic condition of Tehran, Iran (35°41′N ,51°19′E). Two Plexiglas tanks are used with dimensions of 200 mm × 100 mm with one side made of aluminium sheets with 2 mm thickness. The thermoelectric modules are installed between these two aluminium sheets. On the inside of the tanks, heat sinks were used to raise the heat transfer. The heat sink with a total length of 150 mm and 20 numbers of rectangular fins with variable

Fig. 1. *Photo of the solar still with hot and cold tanks connected to the heat sink*

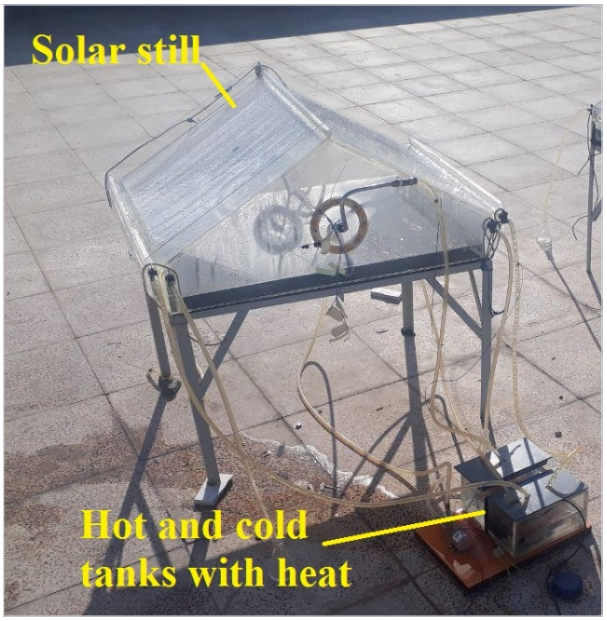

Table 1. *Dimensional parameters of the heat sink*

Parameter	Amount	Dimension	Unit
L	80	Height	mm
W	50	Width	mm
B	150	Length	mm
N	20	Number of fins	No.

spacing depending on optimal thickness (length is constant) of copper was considered (copper was chosen for fins material to have a better heat conduction coefficient). Table 1 specifies the dimensional parameters of the heat sink. The distance between the hot and cold water tanks is covered with insulation to prevent the connection of the hot plate to the cold plate. Fig. 2 shows the drawing of a thermoelectric hot and cold side connected to the heat sink used in the solar still.

Fig. 2. *Schematic model of the heat sink*

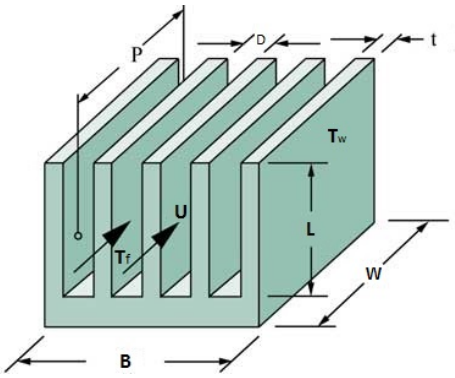

The fins' width is considered fixed and assuming the constant volume for the fins; the optimized dimensionless thickness of the fins can be calculated. As it can be seen in Fig. 2, the fluid flows from around towards the heat sink by forced convection.

One dimensional assumption

The heat sink is considered adiabatic at both ends, and for one dimensional assumption, heat transfer from thin lateral surfaces is neglected and these surfaces are considered insulated. In addition, the base temperature

distribution of the fins along the sink width (W) is considered uniform. Another required assumption for one dimensional heat transfer is to consider half of the sink due to symmetry, assuming the fins' top surfaces to be insulated. Besides, we assume that the flow is laminar and fully developing.

Variables of the study

Eight different cooling nanofluids consisting of aluminium, alumina, titanium, titanium dioxide, copper, copper oxide, iron and iron oxide nanoparticles with water as the base fluid were used in this study. The nanofluids were selected so that performance of a nanofluid with metallic nanoparticles and its oxide nanoparticles could be compared. The nanoparticle diameters of the selected nanofluids were 25, 50 and 75 nm and volume fractions of 1%, 3%, 5%, 7% and 9% were considered and their respective effect on the heat sink fin's optimum thickness was investigated. The average fluid temperatures were considered as 310, 320, 330 and 340 K, the input flow velocity was considered as 5 m/s (for laminar flow) and their effects on the fin's dimensionless optimum thickness were also investigated.

Theoretical background

Fin base temperature Tw is required to calculate convection heat transfer from fin's lateral surfaces, using the Newton law of cooling. On the other hand, the fin's surface distribution temperature can be calculated from a general differential equation using conservation of the energy law for fins with one dimensional assumption. After solving the equations and applying the adiabatic boundary conditions for the fin's tip, the heat transfer rate from the fin's wall with the temperature of Tw to the fin can be obtained by (Bejan, 2013):

$$q_{fin} = M\theta_w \tanh mL \quad (1)$$

where: $m - \sqrt{\frac{hp}{k_w A_c}}$; $M - \sqrt{hpk_w A_c}$; $\Theta_w - T_w - T_f$; AC – cross section area; p – perimeter.

In addition, the k_w and h are conduction and convection heat transfer coefficients, respectively. The efficiency for one fin is defined as follows:

$$\eta = \frac{q_{fin}}{q_{max}} = \frac{\tanh mL}{mL} \quad (2)$$

The total efficiency of the heat sink (group of fins) is achieved by the following relation:

$$\eta_{Heat\ Sink} = \frac{q_{total}}{hA_t\theta_w} = 1 - \frac{NA_c}{A_t}(1-\eta) \quad (3)$$

where: $A_t = NA_c + A_b$–; $A_c = wt$; $P = 2w$

Optimum dimensionless fin thickness

Assuming laminar and developed flow over the flat plate, the average convection heat transfer coefficient in the direction of fin's thickness is obtained by equation (4) (Bejan, 2013):

$$h = Nu\left(\frac{k_f}{D_h}\right) \quad (4)$$

The heat transfer rate per unit length of the fins can be rewritten as follows:

$$q_{fin} = 2hL(T_w - T_f)\eta \quad (5)$$

The coefficient of 2 in equation (5) is for heat transfer from both sides of the fin. For laminar flow between two surfaces with constant temperature in any section, the Nusselt number is constant and equal to 7.54 (Bejan, 2013). Considering that $D_h = 2D$, equation (5) can be rewritten as follows:

$$h = Nu\left(\frac{k_{nf}}{2D}\right) \quad (6)$$

Substituting the value of m in equation (6):

$$h = (Nu\frac{k_{nf}}{k_w})^{1/2}\frac{L}{(tD)^{1/2}} \quad (7)$$

The total number of fins in a heat sink with the length of B is $N = \frac{B}{t+D}$. Therefore, the overall heat transfer can be obtained as follows:

$$q_{total} = \left(\frac{B}{t+D}\right)Nuk_{nf}\frac{L}{D}(T_w - T_f)\eta \quad (8)$$

For simplifying, after normalizing the overall heat transfer equation, the relation of $Q = \frac{q_{total}}{k_w(T_w - T_f)B/L}$ is used. Therefore:

$$Q = Nu\frac{k_{nf}}{k_w}\left(\frac{(\frac{L}{D})^{1/2}}{(1+\frac{t}{D})}\right)\eta \quad (9)$$

Substituting the efficiency of one fin by $\eta = \frac{tanh\, mL}{mL}$ relation, equation (9) can be written in the following form:

$$Q = \frac{L}{D}(Nu\frac{k_{nf}}{k_w})^{1/2}\frac{(\frac{t}{D})^{1/2}}{1+\frac{t}{D}}\tanh[\frac{L}{D}((Nu\frac{k_{nf}}{k_w})^{\frac{1}{2}}(\frac{D}{t})^{\frac{1}{2}}] \quad (10)$$

Simplifying the equation (10) gives the following relation:

$$Q = b\frac{x^{1/2}}{1+x}\tanh(\frac{b}{x^{1/2)}}) \quad (11)$$

Where: $b = \frac{L}{D}(Nu\frac{k_{nf}}{k_w})^{1/2}$;

In addition, considering $\frac{k_{nf}}{k_w} \ll 1$, $\frac{L}{D} > 1$, the parameter of b varies between 0.1 to 10 (assuming logical values of L/D, for example, less than 100). In equation (11), the parameter of x is the dimensionless thickness of the fin and is equal to $x = \frac{t}{D}$. The dimensionless thickness of the fin can be optimized assuming other parameters (like b) to be constant. As the range of b is specified, for some values of b in its limitation, the respective amounts of x_{opt} and Q_{max} are calculated and presented in Table 2. Knowing that the parameter of x is always less than 1, the higher values are not presented.

Table 2. *The amounts of heat transfer with variable b*

b	x_{opt}	Q_{max}	η (%)
0.1	0.054	0.0089	0.945
0.2	0.113	0.0322	0.896
0.5	0.27	0.152	0.7750
1	0.498	0.419	0.627
2	0.809	0.971	0.439
4	0.989	1.999	0.248
10	0.999	5	0.1

Table 2 shows that the maximum heat transfers for b ≥ 2 is obtained when the optimized fin thickness is about 0.8D to D which is not correct due to narrowing the flow passage. Assuming the value of t/D < 0.5 for a logical flow passage, then the value of b shall be b ≤ 1. For this limitation of b, the amount of $\frac{x_{opt}}{b} = 0.054$ is always constant. Therefore, the optimized dimensionless thickness can be written as follows:

$$\frac{t_{opt}}{L} = 0.054(Nu\frac{k_{nf}}{k_w})^{1/2} \quad (12)$$

Cost of water production in solar still

The economic analysis plays an important role in evaluating the performance of a solar still. The capital recovery factor is calculated from the following relation (Rahbar et al., 2017):

$$CRF = \frac{i(1+i)^n}{(1+i)^n - 1} \quad (13)$$

where *i* represents the interest rate, which is 20% in Iran, and *n* indicates the life time of a solar still, which is assumed 20 years in this research. The first annual cost of the solar still is given by Shoeibi et al. (2021):

$$FAC = P \times CRF \quad (14)$$

Where P is the capital cost of solar still. The first annual salvage value (ASV) of solar still is calculated from the following equation (Saini, Sahota, Jain, and Tiwari, 2019):

$$ASV = S \times SSF \quad (15)$$

where S demonstrates the salvage value of the solar still and is usually considered equal to 20% of the capital cost (S = 0.2P) (Shoeibi et al., 2020). The sinking fund factor is calculated by Rahbar and Esfahani (2012):

$$SSF = \frac{i}{(1+i)^n - 1} \quad (16)$$

The annual maintenance cost includes the annual costs of the destruction of goods, repairs, and operation of the solar still, which is equivalent to 10% of the initial cost and is obtained from the following relation (Shoeibi et al., 2020):

$$AMC = 0.10 \times FAC \quad (17)$$

The total annual cost of the solar still is calculated as follows:

$$UAC = FAC + AMC - ASV \quad (18)$$

According to the annual water production M in the solar still, the cost of water production is given by Shoeibi et al. (2020):

$$CPL = \frac{UAC}{M} \quad (19)$$

Environmental analysis

The electrical energy produced by fossil fuels on a power generation plant, which was harmful to the environment, was used to produce all the parts used in the body, electrical equipment, and nanoparticles in the solar still. A large amount of environmental pollutants in the production of these parts are spread to the environment (Rajaseenivasan and Srithar, 2016). The enviroeconomic analysis is specified based on two parameters of carbon dioxide emission and carbon dioxide mitigation.

Carbon dioxide emission

The CO_2 emission per kilowatt-hour is about 0.96 kg (Sovacool, 2008). Meanwhile, the CO_2 production per kilowatt-hour is usually about 2 kg, considering the transmission loss (20%) and distribution loss (40%), which are generally caused by unsuitable equipment. The annual carbon dioxide emission and carbon dioxide emission over the life of the solar still are determined as follows (Dwivedi and Tiwari, 2010):

$$\text{Annual carbon dioxide emission} = \frac{2\times E_{in}}{n} \quad (20)$$

$$\text{Carbon dioxide emission during life time} = 2 \times E_{in} \quad (21)$$

Carbon dioxide mitigation

The annual CO_2 mitigation rate in the solar still (kg/year CO_2) is equal to $(E_{en})_{out}\times 2$. Therefore, the carbon dioxide mitigation during the life of the solar still is $(E_{en})_{out}\times 2\times n$. The net amount of CO_2 mitigation per ton is equal to the CO_2 mitigation minus the CO_2 emission during the life of the solar still, which is determined from the following equation (Joshi and Tiwari, 2018):

$$X_{co_2} = \frac{2\left((E_{en})_{out} \times n - E_{in}\right)}{1000} \quad (22)$$

Where: X_{CO_2} = environmental parameter; $(E_{en})_{out}$ = annual energy output.

Enviroeconomic analysis

The enviroeconomic parameter is equal to the price obtained from CO_2 mitigation over the life of the solar still. The following equation is used to obtain the enviroeconomic parameter (Caliskan, 2017; Shoeibi et al., 2021):

$$Z_{co_2} = z_{co_2} \times X_{co_2} \quad (23)$$

Where: Z_{CO_2} = enviroeconomic parameter; z_{CO_2} = international carbon cost (14.5$ per ton CO_2).

Exergoenvironmental analysis

Since water productivity requires the consumption of energy from fossil fuels and this energy source pollutes the environment, the water production from renewable sources will reduce this level of pollution. The exergoenvironmental parameter is used to reduce carbon dioxide by various solar stills, based on the annual exergy output. The following equation can be applied to assess exergoenvironmental analysis during the life of a solar still (Shoeibi et al., 2021):

$$X_{ex,co_2} = \frac{2\left((E_{ex})_{out}\times n - E_{in}\right)}{1000} \quad (24)$$

Where: X_{ex,co_2} = exergoenvironmental parameter; $(E_{ex})_{out}$ = annual exergy output.

Exergoenviroeconomic analysis

The exergoenviroeconomic analysis is a method to evaluate the price resulting from CO_2 emissions based on exergy and is calculated from the following equation (Elbar et al., 2019):

$$Z_{ex,co_2} = z_{co_2} \times X_{x,co_2} \quad (25)$$

Calculation of nanofluid thermal conductivity

The equations of heat sink with the nanofluid are the same as the equations with the base fluid, and the density, thermal conductivity, and heat capacity of nanofluids are considered. Table 3 presents the thermal conductivity and density of various nanoparticles. The density of the nanofluid is calculated using the following equation (Kabeel et al., 2017):

$$\rho_{nf} = (1 - \varphi_v)\rho_{bf} + \rho_p\varphi_v \quad (26)$$

Where: φ_v = volume fraction; ρ_p = density of nanoparticles; ρ_{bf} = water density.

The volume fraction of nanofluids can be obtained from the following equation (Chen et al., 2017):

Table 3. *Thermo-physical properties of nanoparticles (Sahota et al., 2020; Sahota and Tiwari, 2017)*

Cu	CuO	Al	Al_2O_3	Ti	TiO_2	Fe	Fe_2O_3	Properties
400	20	237	40	22.5	8.95	72.7	6	$k\ (\frac{W}{m.K})$
8933	6500	2700	3970	4507	4157	7800	5200	$\rho(\frac{Kg}{m^3})$

$$\varphi_v = \left(\frac{\frac{m_n}{\rho_n}}{\frac{m_n}{\rho_n}+\frac{m_b}{\rho_{bf}}}\right) \quad (27)$$

Where: m_n = nanoparticles mass; m_b = water mass; ρ_n = nanoparticle density.

The thermal conductivity of the nanofluid is calculated from the following equation (Kabeel et al., 2017):

$$k_{nf} = k_{bf}\left[\frac{k_p + 2k_{bf} + 2\varphi_v(k_p - k_{bf})}{k_p + 2k_{bf} - \varphi_v(k_p - k_{bf})}\right] \quad (28)$$

Where: k_{bf} = thermal conductivity of water; k_{nf} = thermal conductivity of nanofluid.

The thermal capacity of the nanofluid is obtained from the following equation (Xuan and Roetzel, 2000):

$$(\rho Cp)_{nf} = (1-\varphi_v)(\rho Cp)_{bf} + (\rho Cp)_p \varphi_v \quad (29)$$

Where: Cp_p = thermal capacity of nanoparticles; Cp_{bf} = thermal capacity of water.

The thermal conductivity of the base fluid (water) is obtained by (Nieto de Castro et al., 1986):

$$K_{bf} = 0.6067\left[-1.26523 + 3.704\left(\frac{T_{ave}}{298.15}\right) - 1.43955\left(\frac{T_{ave}}{298.15}\right)^2\right] \quad (30)$$

Discussion and results

The optimum dimensionless fin thickness

Comparison of optimum dimensionless thickness of fins in the heat sink for various nanofluids in different volume fractions, different diameters of nanoparticles and various average temperatures is presented in this part, considering constant width and length of fins. Besides, the optimum volume fraction for each nanofluid is investigated.

Fig. 3 presents the effect of volume fraction percentage of various nanofluids on the optimum thickness of fins in the heat sink with an average temperature of 310 K and nanoparticle diameter of 25 nm. The results from Fig. 3 show that in the volume fractions of 1% to 9%, the lowest thickness is related to aluminium (0.0076) in the volume fraction of 1% and the maximum value of thickness is related to copper nanofluid that has the value of 0.026 in volume fractions of 9%. It can be concluded that minimum optimum dimensionless thickness is related to the nanoparticles which have the minimum density and maximum thermal conductivity.

Fig. 3. *The optimum fin thickness in different volume fractions with a constant nanoparticle size and an average temperature*

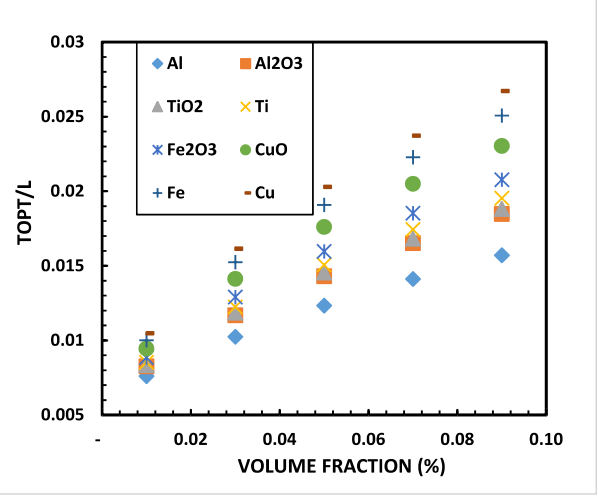

The optimum dimensionless thickness of fins for copper and iron nanofluids is higher than for their respective oxides, while for aluminium oxide, it is calculated higher than aluminium nanofluid. The optimum dimensionless thickness of fins for titanium and titanium oxide nanofluids is approximately equal. It is observed that in all volume fractions the optimum dimensionless thickness for Ti-water, Al_2O_3-water

and TiO_2-water nanofluids is obtained approximately in the same range. With an increment in the volume fraction, the optimum dimensionless thickness of fins increases. Furthermore, the increasing slopes of various nanofluids are different so that the maximum and the minimum slopes are related to copper and aluminium nanofluids, respectively.

In Fig. 4, the optimum dimensionless thickness of fins at an average temperature of 310 K and the volume fraction of 5% for different nanoparticle diameters is compared and evaluated. As it can be seen, by enhancement in the nanoparticles diameter, the optimum dimensionless thickness of fins decreases for various nanofluids. By increasing the particle size, thermal conductivity of nanofluids decreases and the optimum dimensionless thickness of fins is reduced due to an increasing nanoparticles diameter. In addition, the slope of decreasing optimum dimensionless thickness with an increasing nanoparticle diameter for various nanofluids is almost constant.

Fig. 4. *The optimum fin thickness in different nanoparticle sizes with a constant volume fraction and average temperature*

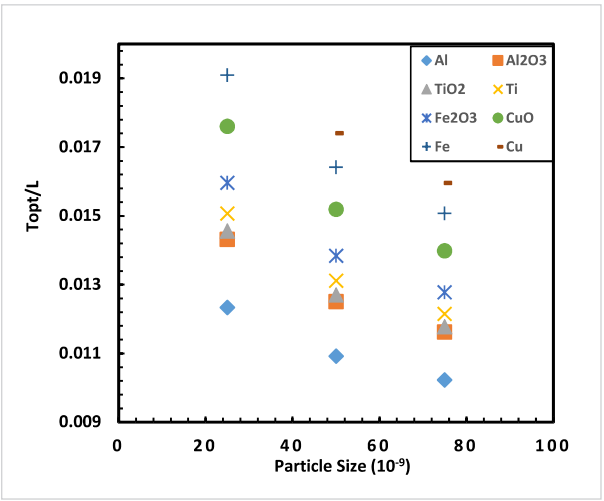

In Fig. 5, the effect of various average temperatures of nanofluids (310, 320, 330 and 340 K) that flow through fins is investigated. It is observed from this figure that by increasing the input flow temperature, the optimum dimensionless thickness of fins increases and the increasing slopes for different nanofluids are almost the same. Increasing the temperature causes an increase in the thermal conductivity and the optimum dimensionless thickness of fins. Furthermore, by temperature variations, the calculated optimum dimensionless thicknesses for alumina and titanium oxide nanofluids is the same. Therefore, in a flow with a low temperature, lower optimum thickness can be selected for all nanofluids which leads to less material consumption.

Fig. 5. *The optimum fin thickness at different average temperatures with a constant volume fraction and nanoparticle size*

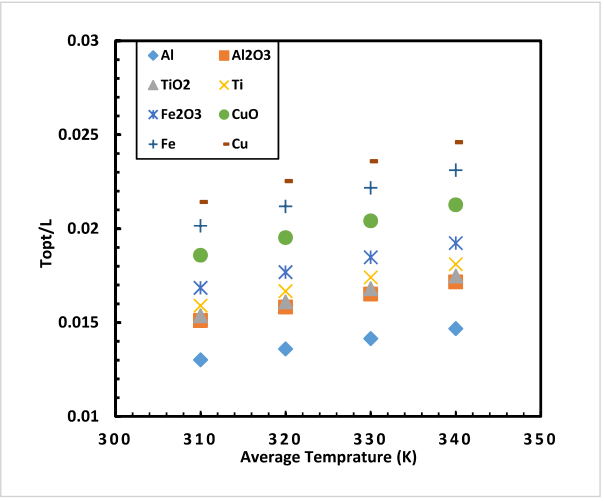

Fig. 6 presents a forced convection heat transfer coefficient for various nanofluids in different volume fractions (1% to 9%). It is observed that the convection heat

Fig. 6. *The heat transfer coefficient of fins in different volume fractions with a constant nanoparticles size and average temperature*

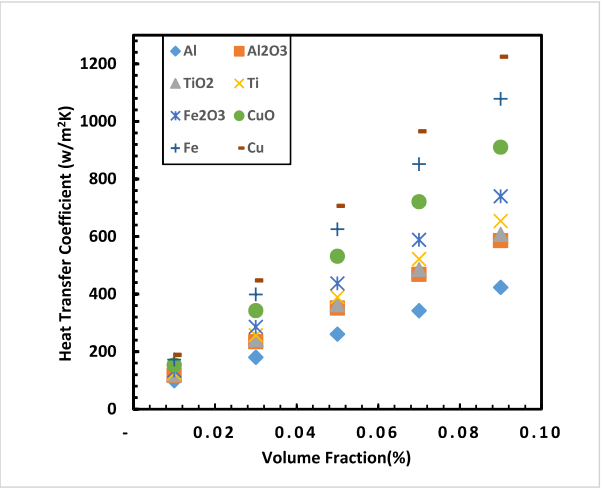

transfer coefficients for various nanofluids in a volume fraction of 0.1% are in the same region. By increasing volume fractions, the slope of a convection heat transfer coefficient for different nanofluids varies so that, in a volume fraction of 9%, copper has the most heat transfer coefficient of 1224 W/m^2 K and copper oxide has the value of 910 W/m^2 K. Besides, aluminium has the least heat transfer coefficient of 423 W/m^2 K and alumina has the value of 585 W/m^2 K. It is observed that only for aluminium nanoparticles the heat transfer coefficient is lower than the amount for its oxide nanoparticles (alumina). Although a high volume fraction results in high optimum thickness and material consumption, it leads to the highest heat transfer coefficient.

The efficiency of fins and heat sink

Figs. 7 and 8, respectively, present the effect of a volume fraction and a nanoparticle diameter on the efficiency of one fin in the optimum dimensionless thickness with an average temperature of 310 K for different nanofluids. Observing these figures, it can be seen that the efficiency of the fin is reduce by enhancement in a volume fraction so that the minimum efficiency of 74.2% is obtained in the copper nanofluid with a 9% volume fraction. Increasing the nanoparticle diameter leads to enhancement in the efficiency of the fin, so that the highest efficiency of 79.1% is obtained in a nanoparticle diameter of 25×10^{-9} for the copper nanofluid. Furthermore, by

Fig. 8. *The efficiency of the fin in different nanoparticle sizes with a constant volume fraction and average temperature*

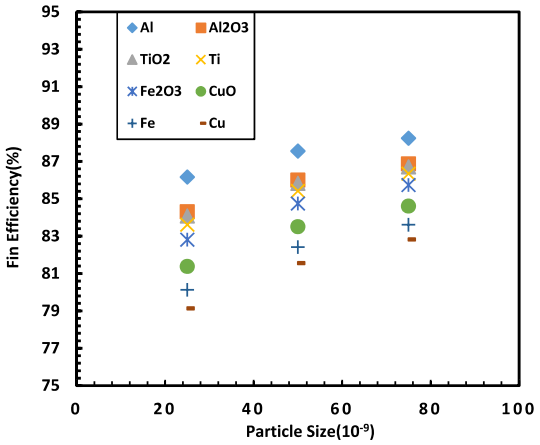

increasing nanoparticle diameters, the efficiency of one fin is increased. It is also observed that the slopes of the efficiencies are different for various volume fractions and nanoparticle diameters. For the copper nanofluid, the highest efficiency loss results from increasing the volume fraction, while for the aluminium nanofluid, the lowest effect on the efficiency is observed by volume fraction variations. This effect is valid for nanoparticle diameter variations, too.

Fig. 9 presents the efficiency of the heat sink in the optimum dimensionless thickness for various volume

Fig. 7. *The efficiency of the fin in different volume fractions with a constant nanoparticles size and average temperature*

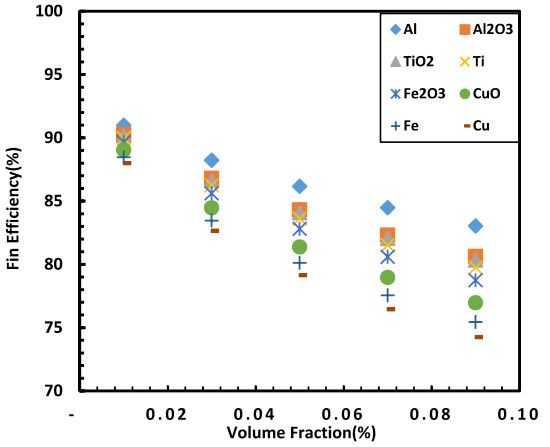

Fig. 9. *The efficiency of the heat sink in different volume fractions with a constant nanoparticles size and average temperature*

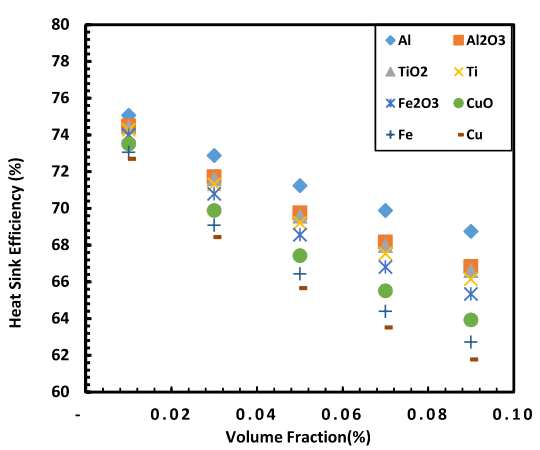

fractions (1% to 9%) with the nanoparticle diameter of 25 nm and the average temperature of 310 K. The effect of nanoparticle diameter variations (25 to 75 nm) is investigated in Fig. 10 with a volume fraction of 5% and an average temperature of 310 K of different nanofluids. The efficiency of the heat sink, same as for one fin, is reduced by increasing the volume fraction and is enhanced by increasing nanoparticle diameters; the efficiency of the heat sink is decreased.

Fig. 10. *The efficiency of the heat sink in different nanoparticle sizes with a constant volume fraction and average temperature*

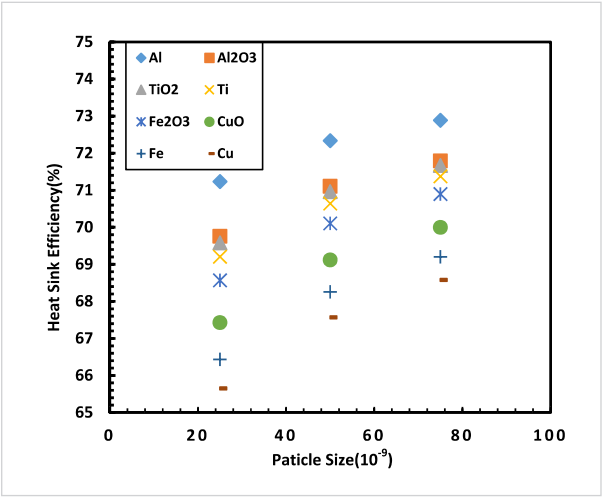

Environmental analysis

Table 4 presents the construction cost of thermoelectric solar desalination. The results show that the cost of fabrication of a thermoelectric solar still is equal to 281 $. Table 5 shows the cost of water productivity with interest rate of 20% and life time of 20 years in the solar still. The results show that the cost of water production in the solar still is equal to 0.0699 $/l/m^2.

Table 6 shows the embodied energy of solar stills. The energy used to produce different components in the solar still is about 185.8 kWh. Due to the lack of information about the thermoelectric production process, we do not considered the embodied energy of the thermoelectric module (Parsa et al., 2020).

Table 7 shows the environmental, enviroeconomic, exergoenvironmental and exergoenviroeconomic parameters for 20 years life time in the thermoelectric solar still. It can be seen that the CO_2 emissions depend on the embodied energy. The carbon dioxide mitigation based on the environmental parameter and exergoenvironmental parameters in the solar still are about 23.78 tons of CO_2 and 1.04 tons of CO_2, respectively. Moreover, the enviroeconomic parameter and exergoenviroeconomic parameters in the solar still were about 344.79 $ and 15.02 $, respectively.

Table 4. *Construction cost of the thermoelectric solar still*

Components	Cost of the thermoelectric solar still ($)	Salvage value ($)
Thermoelectric solar still		
Plexiglas	180	36
Pumps	20	4
Thermoelectric module	30	6
Galvanized support	15	3
Heat sink	20	4
PVC pipe	4	0.8
Aluminium sheet	7	1.4
Nut and bolt	5	1
Total cost	281	56.2

Table 5. *Cost analysis of solar stills with different life times and interest rates*

Type of solar still	n (year)	i (%)	CRF	FAC	SFF	S	ASV	AMC	UAC	M ($l/m^2.year$)	CPL ($\$/l/m^2$)
Thermoelectric solar still	20	0.20	0.200	18.613	0.005	18.6	0.003	2.79	21.402	945	0.0699

Table 6. *Embodied energy of different components of solar stills (Sahota et al., 2017; Yousef and Hassan, 2019)*

Type of solar still	Components	Energy density		Mass of component (kg)	Embodied energy (kWh)
		MJ/kg	kWh/kg		
Thermoelectric solar still	Glass	31.5	28.3	2	56.6
	pump (PVC)	77.2	21.4	0.1	2.14
	Heat sink (copper)	100	27.7	0.2	5.5
	Aluminium sheet	199	55.2	0.3	16.5
	Body (steel)	25	6.9	5.5	38.2
	Hot reservoir (Plexiglass)	102	28.3	0.5	14.2
	Insulation	55.6	15.44	0.3	4.63
	Pipe (PVC)	77.2	21.4	0.3	6.4
	Support (galvanized)	50	13.9	3	41.7
	Total embodied energy (kWh)	-	-	-	185.8

Table 7. *Environmental and enviroeconomic parameter for the thermoelectric solar still*

Parameter	Thermoelectric solar still
Life time (years)	20
Embodied energy (kWh)	185.8
Annual energy output (kWh)	603.7
Annual exergy output (kWh)	35.19
Carbon dioxide emission during life time (kg)	371.6
Carbon dioxide mitigation during life time (ton Co_2)	24.15
Environmental parameter (ton Co_2)	23.78
Enviroeconomic parameter ($)	344.79
Exergoenvironmental parameter (ton)	1.04
Exergoenviroeconomic parameter ($)	15.02

Conclusion

In this paper, a mathematical analysis was performed to optimize the geometry of fin thickness in a heat sink used in the thermoelectric cold and hot sides of the solar still, applying nanofluids of aluminium, alumina, titanium, titanium dioxide, copper, copper oxide, iron and iron oxide with water as the base fluid. Furthermore, the effect of volume fraction, nanoparticle diameter and average temperature of nanofluid flow was investigated on optimization of the fins' section geometry. The summary of the most important results is as follows:

- By increasing nanoparticle diameters at a constant volume fraction, the optimum dimensionless thickness of the fin is reduced for various types of nanofluids and the slope of optimum dimensionless thickness reduction is different for various nanofluids.
- In a flow with a high temperature, higher optimum thickness is calculated for all nanofluids, which leads to more material consumption.
- The highest heat transfer coefficient is obtained for copper and the lowest is obtained for aluminium.
- The enviroeconomic parameter and exergoenviroeconomic parameters in the solar still are about 344.79 $ and 15.02 $, respectively.
- The optimum volume fraction of nanofluids with a 25 nm particle diameter is in the range of 3.95% to 3.65% to minimize the material consumption and maximize the heat transfer coefficient.
- The heat sink thermal efficiency is reduced by increasing the volume fraction and is increased by increasing the nanoparticle diameter.
- The carbon dioxide mitigation based on the environmental parameter and exergoenvironmental parameters in the solar still are about 23.78 tons of CO_2 and 1.04 tons of CO_2, respectively.

Nomenclature

B	lenght of heat sink (m)
C_P	Specific heat capacity (J/g·K)
d_P	Nanoparticle Diameter (m)
h	Covection heat transfer coeffient ($W/m^2 \cdot K$)
K	Coduction heat transfer coeffient (W/m·K)
D	Space between fin (m)
K_B	Steffan Boltzman Constant
E_{in}	Embodied energy (kWh)
$(E_{en})_{out}$	Annual energy output (kWh)
$(E_{ex})_{out}$	Annual exergy output (kWh)
X_{co_2}	Environmental parameter (Ton Co_2)
X_{ex,co_2}	Exergoenvironmental parameter (Ton Co_2)
L	height of heat sink (m)
Nu	Nusselt number
A_t	Total area of heat sink (m^2)
A_c	Area of fin (m^2)
A_b	Are of heat sink without fin (m^2)
q_{fin}	Heat transfer of fin (W)
T_w	Tepmprature of heat sink (K)
T_f	Temprature of fluid (k)
t_{opt}	Optimum thickness of fin (m)
η	Efficiency of fin
$\eta_{Heat\ sink}$	Efficiency of heat sink
π	Pi number
ρ	Density (Kg/m^3)
ϕ	Volume fraction

References

Bejan, A. 2013. Convection heat transfer: John wiley and sons. https://doi.org/10.1002/9781118671627

Caliskan, H. 2017. Energy, exergy, environmental, enviroeconomic, exergoenvironmental (EXEN) and exergoenviroeconomic (EXENEC) analyses of solar collectors. Renewable and Sustainable Energy Reviews, 69: 488-492. https://doi.org/10.1016/j.rser.2016.11.203

Chen, W., Zou, C., Li, X., Li, L. 2017. Experimental investigation of SiC nanofluids for solar distillation system: Stability, optical properties and thermal conductivity with saline water-based

fluid. International Journal of Heat and Mass Transfer, 107: 264-270. https://doi.org/10.1016/j.ijheatmasstransfer.2016.11.048

Dwivedi, V. K., Tiwari, G. N. 2010. Thermal modeling and carbon credit earned of a double slope passive solar still. Desalination and Water Treatment, 13(1-3): 400-410. https://doi.org/10.5004/dwt.2010.856

Elbar, A. R. A., Yousef, M. S., Hassan, H. 2019. Energy, exergy, exergoeconomic and enviroeconomic (4E) evaluation of a new integration of solar still with photovoltaic panel. Journal of Cleaner Production, 233: 665-680. https://doi.org/10.1016/j.jclepro.2019.06.111

Joshi, P., Tiwari, G. N. 2018. Energy matrices, exergo-economic and enviro-economic analysis of an active single slope solar still integrated with a heat exchanger: A comparative study. Desalination, 443: 85-98. https://doi.org/10.1016/j.desal.2018.05.012

Kabeel, A. E., Omara, Z. M., Essa, F. A. 2017. Numerical investigation of modified solar still using nanofluids and external condenser. Journal of the Taiwan Institute of Chemical Engineers, 75: 77-86. https://doi.org/10.1016/j.jtice.2017.01.017

Nieto de Castro, C., Li, S., Nagashima, A., Trengove, R., Wakeham, W. 1986. Standard reference data for the thermal conductivity of liquids. Journal of physical and chemical reference data, 15(3): 1073-1086. https://doi.org/10.1063/1.555758

Parsa, S. M., Rahbar, A., Javadi Y, D., Koleini, M. H., Afrand, M., Amidpour, M. 2020. Energy-matrices, exergy, economic, environmental, exergoeconomic, enviroeconomic, and heat transfer (6E/HT) analysis of two passive/active solar still water desalination nearly 4000m: Altitude concept. Journal of Cleaner Production: 121243. https://doi.org/10.1016/j.jclepro.2020.121243

Rahbar, N., Esfahani, J. A. 2012. Experimental study of a novel portable solar still by utilizing the heatpipe and thermoelectric module. Desalination, 284: 55-61. https://doi.org/10.1016/j.desal.2011.08.036

Rahbar, N., Gharaiian, A., Rashidi, S. 2017. Exergy and economic analysis for a double slope solar still equipped by thermoelectric heating modules - an experimental investigation. Desalination, 420: 106-113. https://doi.org/10.1016/j.desal.2017.07.005

Rajaseenivasan, T., Srithar, K. 2016. Performance investigation on solar still with circular and square fins in basin with CO2 mitigation and economic analysis. Desalination, 380: 66-74. https://doi.org/10.1016/j.desal.2015.11.025

Sahota, L., Arora, S., Singh, H. P., Sahoo, G. 2020. Thermo-physical characteristics of passive double slope solar still loaded with MWCNTs and Al2O3-water based nanofluid. Materials Today: Proceedings. https://doi.org/10.1016/j.matpr.2020.01.600

Sahota, L., Shyam, Tiwari, G. N. 2017. Energy matrices, enviro-economic and exergoeconomic analysis of passive double slope solar still with water based nanofluids. Desalination, 409: 66-79. https://doi.org/10.1016/j.desal.2017.01.012

Sahota, L., Tiwari, G. N. 2017. Exergoeconomic and enviroeconomic analyses of hybrid double slope solar still loaded with nanofluids. Energy Conversion and Management, 148: 413-430. https://doi.org/10.1016/j.enconman.2017.05.068

Saini, V., Sahota, L., Jain, V. K., Tiwari, G. N. 2019. Performance and cost analysis of a modified built-in-passive condenser and semitransparent photovoltaic module integrated passive solar distillation system. Journal of Energy Storage, 24: 100809. https://doi.org/10.1016/j.est.2019.100809

Shoeibi, S., Rahbar, N., Abedini Esfahlani, A., Kargarsharifabad, H. 2020. Application of simultaneous thermoelectric cooling and heating to improve the performance of a solar still: An experimental study and exergy analysis. Applied Energy, 263: 114581. https://doi.org/10.1016/j.apenergy.2020.114581

Shoeibi, S., Rahbar, N., Esfahlani, A. A., Kargarsharifabad, H. 2021. Energy matrices, exergoeconomic and enviroeconomic analysis of air-cooled and water-cooled solar still: Experimental investigation and numerical simulation. Renewable Energy, 171: 227-244. https://doi.org/10.1016/j.renene.2021.02.081

Sovacool, B. K. 2008. Valuing the greenhouse gas emissions from nuclear power: A critical survey. Energy Policy, 36(8): 2950-2963. https://doi.org/10.1016/j.enpol.2008.04.017

Xuan, Y., Roetzel, W. 2000. Conceptions for heat transfer correlation of nanofluids. International Journal of Heat and Mass Transfer, 43(19): 3701-3707. https://doi.org/10.1016/S0017-9310(99)00369-5

Yousef, M. S., Hassan, H. 2019. Assessment of different passive solar stills via exergoeconomic, exergoenvironmental, and exergoenviroeconomic approaches: A comparative study. Solar Energy, 182: 316-331. https://doi.org/10.1016/j.solener.2019.02.042